Int. Journ. of Wettability Science and Technology, Vol. 1, pp. 47–62
Reprints available directly from the publisher.
Photocopying permitted by license only.

Anisotropic Spreading Along the Textured Surfaces with Isotropic Wetting

A.M. EMELYANENKO*, L.B. BOINOVICH AND K.A. EMELYANENKO

A.N. Frumkin Institute of Physical Chemistry and Electrochemistry, Russian Academy of Sciences, Leninsky prospect 31 bldg. 4, 119071 Moscow, Russia

Fast spreading of a decane droplet over superoleophilic substrates with multimodal surface roughness and different chemical composition of the top textured layer is studied experimentally. New techniques and software based on digital image processing of high spatial resolution optical images of a spreading droplet developed in this study allowed one to distinguish 3 spreading fronts propagating along the substrate with multimodal roughness. It was found that the spreading velocities for bulk droplet base, for the front associated with the propagation of liquid over microchannels/microgrooves, and for the nanotexture impregnation are significantly differed from each other. An important new feature of spreading obtained in this study is related to anisotropic spreading for the latter two fronts at the simultaneous isotropic spreading of bulk drop base. The analysis of obtained experimental data for spreading of the decane droplet over the superoleophilic substrates with different chemical composition indicates that the spreading velocity is affected by the Young (local three-phase) contact angle, established in the course of spreading of liquid along the rough/textured substrate.

Keywords: Wettability, surface roughness, spreading kinetics, decane, superhydrophobic surfaces, superoleophilic surfaces, microtexture, nanotexture

1 INTRODUCTION

Modification of the surface targeted on controlling wettability and liquid spreading is a very active direction of research [1-13] not only for a purely scientific reason but also because of significant interest for a broad range of

*Corresponding author: E-mail: ame@phyche.ac.ru

applications, including surface coating, printing, painting, lab-on-a-chip technologies, composite manufacturing, microfluidics, etc. One of the most intensively developed areas in the manufacturing of functional materials is the creation of coatings with the ultrafast spreading of a number of liquids along the surface of coatings with the formation of uniform wetting layers [14-19]. Generally, one can control the wetting by and spreading of a given liquid over a surface by modifying either the chemistry or the topology of top surface layers. The rapid progress of recent decades in the technologies of micro- and nanoprocessing of the surfaces has provided ample opportunities for varying the surface properties and creating the required surface patterns or structures. Designing such surfaces is a complex scientific and technical problem. The surfaces with multimodal roughness based on nano- and micro-elements of the texture, which are chemically modified to impart wetting with test liquids are considered as the most promising for control of spreading peculiarities and velocity. Numerous experimental and theoretical studies were performed for the analysis of spreading of Newtonian liquids along the smooth substrates [3, 12, 14, 18, 20]. It was shown that inertial, gravitation and capillary effect act as driving forces for the spreading of the bulk part of the droplet, while the viscous effects and solid/liquid friction effect associated with the interaction between the molecules of a spreading liquid and the substrate counterpoise the driving force and control the spreading rate. The spreading of the precursor film, which is typically constituted by a few molecular layers, is mainly ruled by the surface forces, at the same time, viscous and friction effects resist it. Theoretical consideration of spreading along the smooth surfaces provides a qualitative description of bulk droplet/precursor film radius on time by power-law time dependences with different exponents at different time scales of the spreading process [3, 19-29].

The situation becomes far more complicated for the case of spreading over roughened surfaces [30-33]. Micro- and nano-sized topographic features form multiple capillary channels with different capillary pressures, impregnation of which is determined by the complex interplay of gravitational contributions, capillary forces, surface forces and viscous/friction dissipation. Therefore, despite the large number of papers, in which the spreading of various liquids over substrates was studied by both real experiments and numerical simulations, a more detailed understanding of the processes determining the behavior of liquid droplets in contact with textured, rough or porous solid surfaces is still highly demanded. Even with the importance of spreading over textured surfaces for many practical applications, the rigorous theoretical and experimental studies in this domain are still very scarce. The necessity to find the joint self-consistent solution of equations describing the behavior of bulk part of the droplet over the substrate, with the equations of liquid penetration inside the cavities and grooves within the surface texture leads to significant complication of a posed theoretical problem. However, apart from the fundamental understanding of spreading/imbibition problem,

many practical applications require the knowledge of the rates of wetting processes. Particularly, one is often interested to know how fast a liquid, deposited on a solid textured substrate, can spread over a given area and what are the key physicochemical parameters which control the spreading rate and the structure of newly formed liquid layer. For a better understanding of above problem, experimental studies of the spreading of a liquid decane droplet over the substrates with similar multimodal surface roughness subjected to treatment with different chemical modifiers are carried out in this work. Throughout this work, the textured substrates, which are characterized macroscopically by isotropic wetting, show well defined anisotropic spreading behavior.

2 MATERIALS AND METHODS

2.1 Materials

N-decane (•99.5%) and stearic acid (grade 1, •98.5%) were purchased from Sigma-Aldrich, Inc. and used without further purification. Methoxy- {3-[(2,2, 3,3,4,4,5,5,6,6,7,7,8,8,8- pentadecafluorooctyl)-oxy]-propyl}-silane were synthetic samples supplied by Prof. Aziz Muzafarov, ISPM RAS. Redistilled ethyl alcohol of chemical grade was used as a solvent for stearic acid. The experiments were performed on laser textured substrates of aluminum-magnesium alloy (AMG3, an analogue of 5754 alloy according to International Alloy Designation System, purchased from Neva Metal LLC, Russia) subjected to different types of chemical modification.

2.2 Substrate preparation

Flat sheets (1 mm thick) of AMG3 alloy were cut on samples with dimensions 15×15 mm^2. The smooth reference substrates for spreading experiments were obtained by substrate grinding, followed by diamond paste polishing with the diamond grain sizes sequentially 3 and 1 μm.

Hierarchically textured surfaces of AMG3 were fabricated by nanosecond laser treatment. Prior to such treatment, the samples were degreased in a 1M KOH solution, ultrasonically washed in deionized water and air dried. Laser treatment was performed in ambient conditions with humidity of 40-50% and temperature of 20-25°C.

An infrared laser system (Argent-M; LTC, LLC) with an IR ytterbium fiber laser (wavelength 1.064 μm) was used, which provides a wide choice of laser parameters, with a 2-axis laser beam deflection unit (MS10; Raylase, GmbH). The samples were raster scanned at a linear speed of 50 mm/s with parallel line pitch of 0.02 mm, a pulse duration of 50 ns, the repetition rate of 20 kHz and peak power of 0.95 mJ in TEM_{00} mode. The laser beam diameter was focused into a 40 μm wide (the $1/e^2$ level) focal spot with peak fluence of ≈19 J/cm^2 onto a sample surface. The chosen peak fluence exceeds the abla-

tion threshold leading to intense ablation from the surface at chosen laser beam treatment parameters.

Four different types of AMG3 textured substrates were used for spreading experiments. All these types of substrates were textured by laser pulses with above-specified parameters and only differed from each other by the method of chemical modification after the laser texturing. The first type (referred to as T-sample) was ultrasonically washed in deionized water and air dried. The second type (T-UV-sample) was ultrasonically washed in deionized water, air dried and then exposed to UV-ozone treatment (Bioforce Labs, Inc) for 60 min, which results in the grafting of surface hydroxyl and carboxyl groups to the surface. The third type (FSi-sample, where FSi stands for fluorooxysilane) after washing in deionized water, drying and UV-ozone-grafting of surface hydroxyl groups to the surface, was exposed to the vapors of methoxy-{3-[(2,2,3,3,4,4,5,5,6,6,7,7,8,8,8-pentadecafluorooctyl)oxy]propyl}-silane at T=95 °C for 1h. Further drying for 1 h in an oven at 130°C, resulted in the formation of a cross-linked layer of fluorooxysilane atop the laser textured surface. The fourth type (SA-sample) was washed and UV-ozone pretreated in a way similar to the preparation of the FSi-sample. However, the chemical modification of the surface of this sample was performed using chemisorption of stearic acid (SA) from 0.05 w.% solution in ethyl alcohol onto the surface hydroxyl groups. Then the samples with stearic acid chemisorbed monolayer were rinsed in ethanol to remove the physically adsorbed molecules and dried for 1 h in an oven at 130 °C.

2.3 Substrate characterization

The morphology of the sample surfaces was studied using a scanning electron microscope (SEM) (Supra 40 VP, Carl Zeiss AG, Ltd). Micrographs were taken at 2-5 kV acceleration voltage using a secondary electron detector.

Characterization of the wettability of used substrates was based on contact and roll-off angle measurements. Digital video image processing of sessile droplets was implemented to analyze the droplet shape parameters. The homemade experimental setup for recording optical images of sessile droplets and the software for subsequent determination of droplet parameters using the Laplace curve fitting routine were described earlier [34, 35]. In order to characterize the wettability of coatings, initial contact angles for 6 μL droplets of water and decane were measured at five different surface locations for each sample.

To measure the roll-off angle for the superhydrophobic surfaces, 10 μL droplets were deposited on the surface. After the initial droplet shape was equilibrated, manipulation with an angular positioner allowed the sample surface tilt to be changed in a controllable manner and detect the roll-off angle by averaging over 10 different droplets on the same substrate.

2.4 Spreading studies

The studies of the spreading kinetics were performed in the conditions of both an open experimental cell and in a saturated vapor pressure atmosphere. The experimental setup for recording optical images of spreading droplets is presented in Figure 1. The setup consisted of a leveling optical table, the substrate with spreading droplet which was placed inside the polystyrene experimental cell with transparent glass cover and the high precision dosing system (LSP01-1A; Longer Precision Pump Co., Ltd) with a long needle. Optical images of a spreading droplet were obtained by an optical microscope Stemi SV11 (Zeiss), captured by high-speed digital camera (FL3-U3-13S2M-CS; Point Grey Research Inc) and stored in the computer. For all experiments, the decane droplets with the volume of 6 μL were used.

The method of digital video image processing was used to define the position of points belonging to different spreading fronts. Here, it is worth noting that the analysis of liquid spreading along the rough substrates with multimodal (hierarchical) roughness allowed three different spreading fronts to be distinguished. The first one with the highest expanding rate was associated with the capillary impregnation of a substrate nanotexture by a precursor film. The second front appears due to the propagation of liquid along the microchannels/microgrooves. This front typically

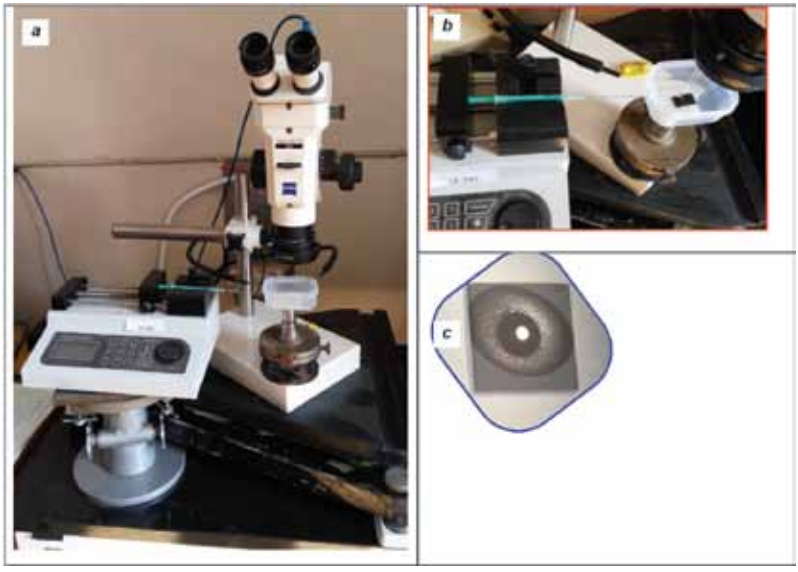

FIGURE 1
Experimental setup for studying spreading of liquid over textured substrates: (a) general view; (b) enlarged image of the dosing syringe and polystyrene experimental cell with a substrate inside; (c) picture of a wet spot on the substrate with a bulk droplet (dark circular area with a bright reflection of the light source in the middle).

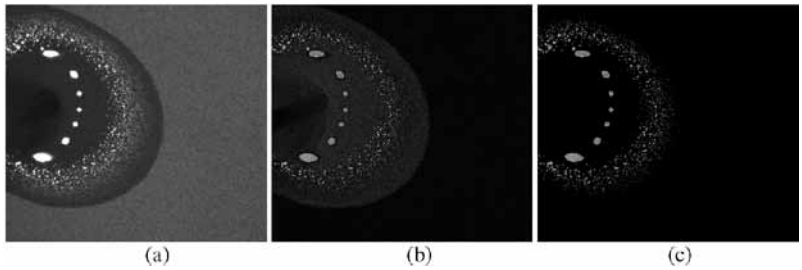

FIGURE 2
Optical image of the spreading decane droplet on the textured substrate (a) and the results of image processing applying different procedures developed in this study: difference filter enhancing the position of outer front of the wet spot (b), and subtraction filter simplifying the detection of bulk droplet base and of the front, associated with the propagation of liquid along the microchannels (c).

has the spreading velocity lower than that for the first one. Finally, the third front was formed by the spreading of a bulk droplet over the rough substrate impregnated with a liquid. The position of each type of abovementioned liquid fronts defined from the analysis of direct (primary) optical image (Figure 2a) was characterized by high noise level due to the roughness of the studied substrates and weak optical contrast in the considered system. To make the detection of a corresponding front position more reliable and less noisy, two types of software procedures for subsequent digital image processing of different fronts were developed. To clarify the applied methods, consider two types of the differential images. The differential image of the first type (Figure 2b) was obtained as a result of the difference in the intensity of scattered light for each pixel in the field of the image for the substrate without droplet and the substrate with the spreading droplet. This type of differential image was applied for reliable positioning of the outer front associated with the capillary impregnation of a substrate nanotexture with a precursor film. The described approach accounts for the depression of light scattering from the nanorough surface upon its filling with a liquid.

The second type of procedure was based on the analysis of differential images (Figure 2c) obtained by pixel-by-pixel subtraction of the intensity of scattered light for the substrate with the spreading droplet and that for the substrate without droplet. This procedure is applicable for digital image processing of front, associated with the propagation of liquid along the microchannels/microgrooves and the front formed by spreading of a bulk droplet base. In this approach, the increase in intensity of reflected light either due to the filling of microchannels with a liquid or due to droplet flattening upon its spreading is accounted for. Two abovementioned software procedures essentially simplified the detection of different spreading fronts by applying the digital image processing to the evolution of liquid spot on the differential images.

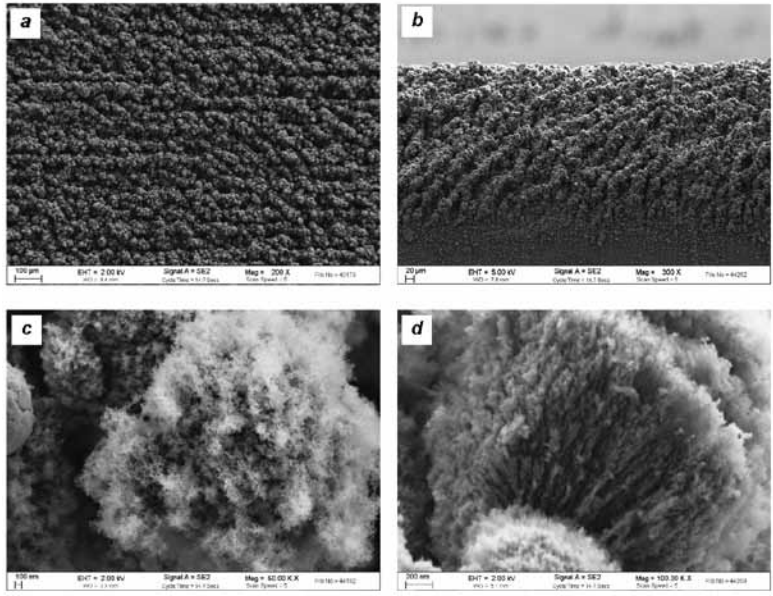

FIGURE 3
Top view (a,c) and cross-section (b,d) SEM images of laser-textured surface of AMG3 samples at different magnifications.

3 RESULTS AND DISCUSSION

The morphology of laser textured substrates used for the study of decane droplet spreading is presented in Figure 3. Top view (a,c) and cross-section (b,d) images at different magnifications clearly illustrate the multimodal roughness of used substrates. The surface texture is characterized by regular surface ripples and trenches (Figure 3a,b), decorated by globule-like aggregates composed of nanoparticles and capsule-shaped pores (Figure 3c,d).

The advancing contact angles measured for polished AMG3 substrates with and without chemical modification and for the textured substrates with and without chemical modification are given in Table 1. Presented data on Young contact angles for both UV-ozone treated and nontreated polished substrates indicate the hydrophilic and oleophilic nature of the aluminum alloy surfaces. In contrast, fluorooxysilane or stearic acid treated polished substrates showed oleophilicity and hydrophobicity. Finally, all the textured substrates are superoleophilic, although FSi-sample and SA-sample are characterized by superhydrophobicity.

It is worth noting that the textured substrates after chemisorption of either the fluorooxysilane or the stearic acid molecules show isotropic wetting with respect to water. This is convincingly proved by an axial symmetry of the sessile water droplets on such surfaces. Besides, the values of roll-off angles

TABLE 1
Typical contact angles for different substrates.

Sample, Treatment	Decane Contact Angle, °	Water Contact Angle, °
Polished untreated	8±3	59.1±1.2
Polished, UV-ozone treated	15±4	86.4±1.4
Fluorooxysilane layer atop of polished substrate	67±2	120.6±1.8
Stearic acid layer atop of polished substrate	<3	118.2±1.9
Laser treated, without chemical modification (T-sample)	0, wicking	0, wicking
Laser treated, UV-ozone treated (T-UV-sample)	0, wicking	0, wicking
Laser treated with fluorooxysilane layer (FSi-sample)	0, wicking	171.2±1.2
Laser treated with stearic acid layer (SA-sample)	0, wicking	169.7±1.6

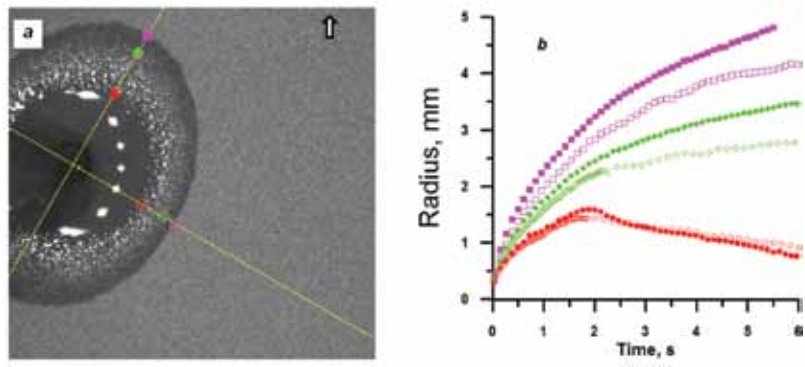

FIGURE 4
Top view of the spreading droplet (a) and time dependences of positions of various spreading fronts (b). The symbols of different color show the instant position of spreading front for bulk droplet base (red color), for spreading along microchannels (green color) and for capillary imbibition into nanotexture (magenta color). The positions of corresponding fronts along the fast/slow axis are shown by filled/empty symbols, respectively. The arrow in (a) indicates the direction of laser scanning.

along the laser texturing direction and normally to this direction were 1.7±1.5° and coincided within the measurement error.

The spreading kinetics of decane droplet on hydrophilic AMG textured substrate is illustrated in Figure 4. The instant top view of the spreading droplet is shown in Figure 4a, while in Figure 4b the variation of the position of three, discussed above, liquid spreading fronts are presented versus spreading time.

The picture of spreading on solids which emerges here indicates anisotropic spreading of the droplet along the rough substrate with multimodal roughness. The direction of fast and slow axes can be easily detected from the

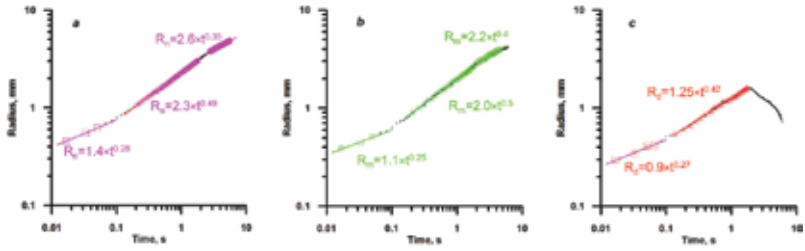

FIGURE 5
Power-law description of the time dependences of the radii of different liquid fronts along the fast axis for spreading of decane on T-sample: (a) impregnation of nanotexture; (b) propagation of liquid along the microchannels; (c) change of the bulk drop base radius. Dots are the experimental points, different symbols are used to distinguish different stages of spreading, and lines are corresponding power-law fits.

image of the liquid spot. It is interesting to note two important features of spreading process. The first one shows that the direction of the fast axis is inclined with respect to the direction of laser scanning along the surface, indicated by an arrow in Figure 4a. These data well correlate with the peculiarities of microtexture of the surface, presented in the cross-section SEM image of the upper part of the textured sample. As follows from Figure 3b, the direction of the effective microgrooves on the surface is not parallel to the scanning direction. The second important feature reveals in the isotropy of spreading of bulk droplet atop of liquid impregnated textured surface at the simultaneous anisotropic spreading of fronts associated with nanoroughness imbibition, shown by magenta curves and propagation of liquid along the microchannels/microgrooves (green curves) (Figure 4b).

The very similar values of the bulk droplet radii for two normal directions once more confirms the axial symmetry of the bulk part of the spreading droplet and the isotropy of wetting. In contrast, the difference in the radii of the outer front associated with nanotexture imbibition during the whole spreading experiment is higher than that for the front associated with microchannels/microgrooves filling. In the early stages, all fronts move away from the droplet center, and the nanotexture imbibition front propagates ahead of two other fronts, showing the highest spreading velocity. The pressure gradient between the bulk droplet and the capillary liquid bridges in both micro- and nanotexture is the main driving force for the spreading, where the excess pressure inside the nanoconfined capillary bridges is defined by both the capillary pressure and the disjoining pressure. Thus, from the highest spreading velocity one can infer the highest pressure gradient for the nanotexture imbibition.

The analysis of the time dependences of the radii of corresponding liquid fronts (Figure 5) shows that the spreading followed three distinct power laws at different stages. The initial stage of the spreading process for all fronts is well approximated by the power-law time dependences $R \sim t^{0.25}$. Such dependence was deduced in the literature [36] basing on the Cox–Voinov equation [23, 37]

which results from the balance between capillary and viscous forces in the liquid wedge and on the assumption of spreading under constant pressure conditions. For the experiments performed in this study, the duration of constant pressure conditions corresponds to the stage of spreading, when the droplet is simultaneously hanging on the dozing system tip and touching the surface. At that stage, the curvature of droplet surface may be considered constant due to the balance of two processes. On the one hand, it is the depletion of droplet volume due to imbibition of liquid into the porous substrate and capillary flow along the microchannels. On the other hand, it is a feeding of the hanging droplet from the reservoir of the dosing system. The detected spreading law was earlier observed for rough surfaces in [30, 36, 38]. However, after approximately 100 ms the droplet detaches from the tip and completely transferred to the substrate, and the second stage of spreading process starts.

The second stage is described by a power law of spreading $R \sim t^k$ with exponent values k close to 1/2. The exponent, characteristic for the capillary impregnation of a substrate nanotexture (Figure 5a) for this stage was 0.49 and for the propagation of liquid along the microchannels (Figure 5b) was 0.50. The spreading of the bulk droplet base (Figure 5c) atop of the textured substrate impregnated with a liquid is well fitted by the dependence $R_d \sim t^{0.42}$. The observed square root time dependences for both the radius of liquid film impregnating the nanotexture and for the radius of liquid flow along the microchannels/microgrooves agree with those predicted by the theoretical consideration. The theoretical analysis, based on the accounting of van der Waals forces, acting in the vicinity of three-phase contact line [24] and becoming the dominant driving force in the liquid front movement, indicates the square root dependence for the thin precursor film spreading. In the case of decane spreading on T-sample, as it was mentioned above, the excess pressure in the film, due to capillary impregnation of a substrate nanotexture, was defined by both van der Waals (dispersion) component of disjoining pressure and the capillary pressure. The role of capillary pressure in the movement of liquid flow inside the grooves was examined both theoretically and experimentally in [31, 39]. In these studies, the hydrodynamic model was proposed which considers Poiseuille flow with the driving force resulting from the pressure drop across a curved liquid/air interface at stationary advancing contact angles. The model showed good agreement with the square root spreading kinetics observed in the experiment. The kinetics of the last stage of spreading is essentially affected by the drop base shrinkage since the bulk droplet is the main source for feeding the liquid content inside the nanotexture and the microchannels/microgrooves.

The exhaustion of the bulk part of the drop volume (the third stage of spreading) leads to slowing down of both the propagation of the front associated with the impregnation of the nanotexture and the propagation of liquid along the microchannels/microgrooves. For the former case, the kinetics of spreading is described by $R_n \sim t^{0.35}$, for the latter $R_m \sim t^{0.4}$.

The analysis of spreading along the slow axis of the substrate demonstrated the similar picture for all spreading fronts at the two first stages: spreading is also well described by the power laws $R \sim t^{0.25}$ for the first stage and $R \sim t^{0.50}$ for the second stage. In contrast, the significant difference for the spreading along slow and fast axis was detected for the third spreading stage, for which evolution of the radii of corresponding fronts along the slow axis is fitted by power laws $R_n \sim t^{0.32}$ and $R_m \sim t^{0.21}$.

Interestingly, analysis of the spreading behavior for water and silicone oil drops on a superhydrophilic micropillar array reported in [30] showed the similar spreading kinetics for the initial stage of bulk drop base propagation and the shrinkage stage. In contrast to results observed here, the kinetics of the micropillar array filling in [30] demonstrated the dependence $R_m \sim t^{0.25}$ for the whole time range.

To check the universality of the obtained spreading laws the spreading kinetics of the decane drop on the chosen substrate with multimodal roughness, subjected to different types of chemical modification, has been monitored. In Figure 6, the data for the radii of fronts associated with the impregnation of the nanotexture on the T-sample (1), T-UV-sample (2), FSi-sample (3), and SA-sample (4) are presented in logarithmic axes for decane spreading along the fast axes. Analysis of these data has shown that for all studied substrates the prolonged second stage of spreading is well described by the power law $R_n \sim t^{0.49 \pm 0.003}$, while the preexponential factors differ from each other. As for the third spreading stage, its analytical description requires the power law $R_n \sim t^{0.37 \pm 0.02}$ with high sensitivity of the preexponential factor to the type of chemical treatment of the textured substrate. It is important to stress here, that four considered substrates at different Young contact angles (measured on finely polished AMG plates, see Table 1), show complete wetting due to multimodal roughness.

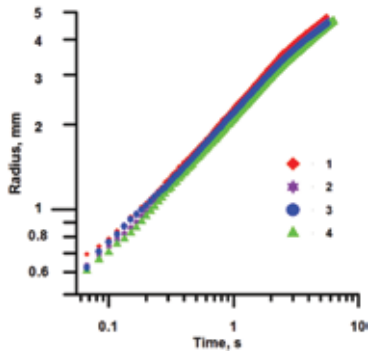

FIGURE 6
The time variation of the radii of fronts associated with the impregnation of the nanotexture along the fast axis on the T-sample (1), T-UV-sample (2), FSi-sample (3), and SA-sample (4).

Wetting of the laser textured substrate after fluorooxysilane layer deposition should be described by Wenzel-Derjaguin equation:

$$\text{Cos } \theta = r \text{ Cos}\theta_Y,$$

where θ and θ_Y are apparent and Young contact angles respectively, and r is a roughness coefficient. Thus, the complete wetting indicates that r is higher than 2 (since $\theta_Y = 67°$, see Table 1). The rough estimation of r value, based on above-discussed argument, looks consistent with the morphology of the surface, presented in Figure 3. To understand in more details the influence of chemical nature of the textured surface, which explicitly affects the Young contact angle of the surface, the spreading kinetics for laser textured substrate without modification and after UV-ozone treatment (Figure 7a) has been compared. The comparison indicates the higher velocity of the radius of propagation for the front associated with the impregnation of the nanotexture on T-sample compared to that for T-UV sample.

One can attribute the higher velocity of nanotexture impregnation front to the lower value of Young contact angle (8˚), measured for polished AMG substrate, versus 15˚, obtained for polished, UV-ozone treated AMG substrate. Having in mind that the local three-phase contact angle, established in the course of spreading of liquid atop of rough/textured substrate, is equal to the Young contact angle for the substrate, the lower value of Young angle results in higher capillary pressure inside the channels/grooves of the texture. Thus, it can be concluded that laser textured AMG substrates demonstrate higher capillary pressure gradient for the spreading decane droplet than that for UV-ozone treated laser textured AMG substrate. To check out this claim, it was reasonable to compare the dynamic contact angles formed by the bulk part of the spreading decane droplet on top of decane impregnated texture for the two considered substrates. In general, the simplest way to do that was to

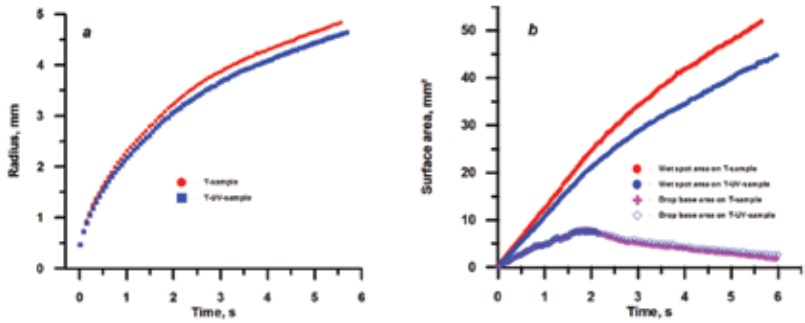

FIGURE 7
The time dependences of the radius of propagation for the front associated with the impregnation of the nanotexture for T-sample and for T-UV-sample (a), and the evolution of corresponding areas for bulk droplet base and wet spot (b).

measure the evolution of instant contact angle, formed by the bulk droplet. To have a good measurement accuracy such studies for the case of low contact angles are generally performed by using the interferometric method. However, for textured substrates studied here, such method is not applicable due to a high level of light scattering from the substrate. Thus, to roughly compare the dynamic contact angles for T-sample and T-UV-sample, the evolution of bulk droplet base area and wet spot area have been analyzed. The latter gives us the area impregnated by liquid. Data, presented in Figure 7b for both substrates indicate the very similar evolution of the areas of bulk droplet base for the droplets spreading for the two substrates. In contrast, during the spreading process, the area of the spot capillary filled with decane for T-UV-sample is essentially lower than for T-sample. Having in mind the same volumes of decane droplet deposited onto both substrates and the similar morphology of both textured substrates one can immediately deduce higher dynamic contact angles on T-UV-sample. That means, according to Wenzel-Derjaguin equation, higher local three-phase contact angle (Young angle) for the T-UV-sample compared to T-sample, that is, poorer wettability of the former. Namely this fact is responsible for the slower spreading kinetics of nanotexture impregnation front for this substrate in comparison to the laser textured substrate without UV-treatment.

The comparison of spreading dynamic of the decane droplets on superoleophilic textured substrates covered by a fluorooxysilane layer or stearic acid layer indicated the similar trend. The higher velocity of spreading of the front associated with capillary impregnation of the nanotexture was observed for the substrate with deposited stearic acid, which showed lower local/Young contact angle.

4 CONCLUSIONS

In this work, spreading of a liquid decane droplet over the superoleophilic substrates with multimodal surface roughness and isotropic wetting was studied experimentally. The experimental setup, based on high resolution optical system and high-speed digital camera was designed for recording optical images of spreading droplets. New techniques and software based on digital image processing developed in this study allowed one to distinguish 3 spreading fronts propagating along the substrate with multimodal roughness. It was found that the spreading velocities for bulk droplet base, for the front associated with the propagation of liquid over microchannels/microgrooves, and for the nanotexture impregnation are significantly different from each other. The analytical description of spreading kinetics allows distinguishing three spreading stages which obey power laws with different exponents. An important new feature of spreading obtained in this study is related to anisotropic spreading for the fronts associated with the propagation of liquid over micro-

channels/microgrooves, and for the nanotexture impregnation at the simultaneous isotropic spreading of bulk drop base. The modification of the chemical composition of the very top textured layer by grafting hydroxyl and carboxyl surface groups or by deposition of hydrophobic molecules like functional silanes or stearic acid, allows one to effectively tune the velocity of liquid spreading without losing the superoleophilic state. The analysis of obtained experimental data for spreading of the decane droplet over the superoleophilic substrates with different chemical composition indicated that the spreading velocity is affected by the Young (local three-phase) contact angle, established in the course of spreading of liquid along the rough/textured substrate. At the same time, such chemical modification leads to a variation of pre-exponential factors for the power law analytical description of the time evolution of spreading front radii, without changing the exponent.

5 ACKNOWLEDGEMENTS

This research was financially supported by the Program for fundamental studies of the Presidium of the Russian Academy of Sciences.

REFERENCES

[1] Daniel R.C. and Berg J.C. Spreading on and penetration into thin, permeable print media: Application to ink-jet printing. *Advances in Colloid and Interface Science* **123** (2006) 439–469.

[2] McHale G., Brown C.V. and Sampara N. Voltage-induced spreading and superspreading of liquids. *Nature Communications* **4** (2006) 1605.

[3] Chen L.Q., Bonaccurso E. and Shanahan M.E.R. Inertial to viscoelastic transition in early drop spreading on soft surfaces. *Langmuir* **29** (2013) 1893–1898.

[4] Viswanath P. and Suresh K.A. Spreading and retraction dynamics of smectic liquid crystal domains at interfaces. *Liquid Crystals* **41** (2014) 320–327.

[5] Lv M., Wang Q., Meng Q., Zhao T., Liu H. and Jiang L. Self-assembly of alumina nanowires into controllable micro-patterns by laser-assisted solvent spreading: towards superwetting surfaces. *CrystEngComm* **17** (2015) 540–545.

[6] Stieghorst J., Majaura D., Wevering H. and Doll T. Toward 3D printing of medical implants: Reduced lateral droplet spreading of silicone rubber under intense IR curing. *ACS Applied Materials & Interfaces* **8** (2016) 8239–8246.

[7] Liu Z., Fang K., Gao H., Liu X. and Zhang J. Effect of cotton fabric pretreatment on drop spreading and colour performance of reactive dye inks. *Coloration Technology* **132** (2016) 407–413.

[8] Das A., Farnham T.A., Subramanyam S.B. and Varanasi K.K. Designing ultra-low hydrate adhesion surfaces by interfacial spreading of water-immiscible barrier films. *ACS Applied Materials & Interfaces* **9** (2017) 21496–21502.

[9] Chen X., Chen J., Ouyang X., Song Y., Xu R. and Jiang P. Water droplet spreading and wicking on nanostructured surfaces. *Langmuir* **33** (2017) 6701–6707.

[10] Strobel M., Kirk S.M., Heinzen L., Mischke E., Lyons C.S., Endle J., Poirier D. and Dillingham G. Contact angle measurements on oxidized polymer surfaces containing water-soluble species. *Journal of Adhesion Science and Technology* **29** (2015) 1483–1507.

[11] Wu C.J., Singh V., Sheng Y.J. and Tsao H.K. Forced spreading of aqueous solutions on zwitterionic sulfobetaine surfaces for rapid evaporation and solute separation. *Langmuir* **33** (2017) 7569–7574.
[12] Choudhury R., Choi J., Yang S., Kim Y.J. and Lee D. Maximum spreading of liquid drop on various substrates with different wettabilities. *Applied Surface Science* **415** (2017) 149–154.
[13] Kubiak K.J., Wilson M.C.T., Mathia T.G. and Carval, P. Wettability versus roughness of engineering surfaces. *Wear* **271** (2011) 523–528.
[14] Ramiasa M., Ralston J., Fetzer R. and Sedev R. The influence of topography on dynamic wetting. *Advances in Colloid and Interface Science* **206** (2014) 275–293.
[15] Wang X., Venzmer J. and Bonaccurso E. Surfactant-enhanced spreading of sessile water drops on polypropylene surfaces. *Langmuir* **32** (2016) 8322–8328.
[16] Theodorakis P.E., Mueller E.A., Craster R.V. and Matar O.K. Superspreading: Mechanisms and molecular design. *Langmuir* **31** (2015) 2304–2309.
[17] McHale G., Shirtcliffe N.J., Aqil S., Perry C.C. and Newton M.I. Topography driven spreading. *Physical Review Letters* **93** (2004) 036102.
[18] Drelich J. and Chibowska D. Spreading kinetics of water drops on self-assembled monolayers of thiols: Significance of inertial effects. *Langmuir* **21** (2005) 7733–7738.
[19] De Coninck J., de Ruijter M.J. and Voué M. Dynamics of wetting. *Current Opinion in Colloid and Interface Science* **6** 49–53.
[20] Cazabat A.M. How does a droplet spread. *Contemporary Physics* **28** (1987) 347–364.
[21] Oron A., Davis S.H. and Bankoff S.G. Long-scale evolution of thin liquid films. *Reviews of Modern Physics* **69** (1997) 931–980.
[22] De Gennes P.G. Wetting: Statics and dynamics. *Reviews of Modern Physics* **57** (1985) 827–863.
[23] Voinov O.V. Hydrodynamics of wetting. *Fluid Dynamics* **11** (1976) 714–721.
[24] Lopez J., Miller C.A. and Ruckenstein E. Spreading kinetics of liquid drops on solids. *Journal of Colloid and Interface Science* **56** (1976) 460–468.
[25] Blake T.D. and de Coninck J. The influence of solid liquid interactions on dynamic wetting. *Advances in Colloid and Interface Science* **96** (2002) 21–36.
[26] Bonn D. Wetting and spreading. *Reviews of Modern Physics* **81** (2009) 739–805.
[27] Findenegg G.H. and Herminghaus S. Wetting: Statics and dynamics. *Current Opinion in Colloid and Interface Science* **2** (1997) 301–307.
[28] Popescu M.N., Oshanin G., Dietrich S. and Cazabat A.M. Precursor films in wetting phenomena. *Journal of Physics-Condensed Matter* **24** (2012) 243102.
[29] Lu G., Wang X.D. and Duan Y.Y. A critical review of dynamic wetting by complex fluids: From newtonian fluids to non-newtonian fluids and nanofluids. *Advances in Colloid and Interface Science* **236** (2016) 43–62.
[30] Kim S.J., Kim J., Moon M.W., Lee K.R. and Kim H.Y. Experimental study of drop spreading on textured superhydrophilic surfaces. *Physics of Fluids* **25** (2013) 092110.
[31] Rye R.R., Mann J.A. and Yost, F.G. The flow of liquids in surface grooves. *Langmuir* **12** (1996) 555–565.
[32] Sekulic D.P. Wetting and spreading of liquid, metals through open microgrooves and surface alterations. *Heat Transfer Engineering* **32** (2011) 648–657.
[33] Joung Y.S. and Buie, C.R. Scaling laws for drop impingement on porous films and papers. *Physical Review E* **89** (2014) 013015.
[34] Emelyanenko A.M. and Boinovich L.B. Application of dynamic thresholding of video images for measuring the interfacial tension of liquids and contact angles. *Instruments and Experimental Techniques* **45** (2002) 44–49.
[35] Emelyanenko A.M. and Boinovich L.B. The role of discretization in video image processing of sessile and pendant drop profiles. *Colloids and Surfaces A: Physicochemical and Engineering Aspects* **189** (2001) 197–202.
[36] Fabie L. and Ondarcuhu T. Writing with liquid using a nanodispenser: spreading dynamics at the sub-micron scale. *Soft Matter* **8** (2012) 4995–5001.
[37] Cox R.G. The dynamics of the spreading of liquids on a solid surface. Part 1. Viscous flow. *Journal of Fluid Mechanics* **168** (1986) 169–194.

[38] Alla H., Freifer S., Talha B.A. and Roques-Carmes, T. New insight into the spreading dynamics of liquids on rough surfaces using computational fluid dynamics. *Russian Chemical Reviews* **82** (2013) 1066–1080.

[39] Mann J.A., Romero L., Rye R.R. and Yost F.G. Flow of simple liquids down narrow V grooves. *Physical Review E* **52** (1995) 3967–3972.